Friction **8**(4): 726–745 (2020)
https://doi.org/10.1007/s40544-017-0299-x
ISSN 2223-7690
CN 10-1237/TH
RESEARCH ARTICLE

Multi-objective optimization of the design parameters of texture bottom profiles in a parallel slider

Nilesh D. HINGAWE*, Skylab P. BHORE

Rotor Dynamics and Vibration Diagnostics Lab, Department of Mechanical Engineering, Motilal Nehru National Institute of Technology Allahabad, Prayagraj 211004, India

Received: 11 October 2018 / Revised: 19 January 2019 / Accepted: 08 May 2019

Abstract: In this paper, a square textured parallel slider is considered for a study to improve the hydrodynamic performance of moving parts. The numerical method is employed for the analysis of a square texture with different bottom profiles: flat, triangle T1, triangle T2, and curved. The governing Reynolds equation is solved using a finite difference numerical discretization technique with the Gauss–Seidel iterative scheme. To obtain optimized process parameters, the response surface methodology-based central composite design along with grey relational analysis multi-objective optimization is used. The multi-objective responses are the load capacity and friction coefficient. The triangle T2 bottom profile yields the highest load capacity and the lowest friction coefficient compared to flat, triangle T1, and curved bottom profiles, of which the triangle T1 bottom profile yields the worst results. For the triangle T2 bottom profile, the flow speed is found to be the most significant process parameter, followed by the aspect ratio. Texture density is found to be the least significant parameter based on increasing the load capacity and decreasing the friction coefficient.

Keywords: texture bottom profile; load capacity; friction coefficient; design of experiment; multi-objective optimization

1 Introduction

Today, energy savings continue to be a heavily researched topic. An extensive amount of energy is consumed to overcome friction, and it is thus desirable to reduce the friction and wear to minimize energy losses and improve the performance of machines. Introducing an intricate shape on either one or both mating surfaces of moving parts helps to enhance their tribological properties. An intentionally produced intricate shape on a surface is called a surface texture. Surface texturing is found to be an effective method to improve the tribological performance of machine components [1]. In fluid film bearings, the surface texture increases the film thickness. The increase in film thickness at the convergent zone generates additional hydrodynamic pressure to further separate the two surfaces. These results increase the load capacity and decrease the local shear stress, and hence reducing the friction [2].

Surface texturing on one of the mating faces in a circumferential gas seal generates a considerable hydrodynamic effect, which maintains a small clearance between the shaft and the seal ring. This prevents them from rubbing against each other, and hence decreases friction and wear [3]. To improve the lubricant quantity in automobile components such as piston rings and wet clutches, the texture geometry acts as micro-pocket. Lubricant retained in the micro-pocket can be released to surrounding areas of the texture to improve the tribological performance of the materials [4, 5]. Adopting a surface texture on the rake face of a cutting tool decreases the tool-chip contact area. Furthermore, debris is trapped in the texture and

* Corresponding author: Nilesh D. HINGAWE, E-mail: rme1603@mnnit.ac.in

Nomenclature

L	Length/ width of unit cell	r	Radius of curved texture
p	Fluid film pressure	N	No. of iterations
p_{cav}	Cavitation pressure	T_d	Texture density
p_a	Atmospheric pressure	A_r	Aspect ratio
h	Nominal film thickness	l	Texture length
h_a	Radial clearance	$q_i^*(k)$	Sequence after data processing
h_b	Texture depth	$q_i(k)$	Comparability sequence
U	Flow speed	$q_0^*(k)$	Reference sequence
μ	Fluid viscosity	Δ_{max}	Global maximum normalized value
τ	Shear stress	Δ_{min}	Global minimum normalized value
W	Load capacity	α	Distinguishing coefficient
F	Friction force	$\xi_i(k)$	Grey relational coefficients
f	Friction coefficient	n	Number of runs

reduction of stiction at the tool-chip interface takes place. This results in a decrease in friction and wear, and hence lesser heat was generated in the cutting tool [6]. In case of an artificial implant, adopting a surface texture decreases the surface contact under boundary lubrication and acts as a lubricant reservoir in elastohydrodynamic lubrication [7].

Surface textures can be fabricated by several conventional and non-conventional machining processes [8]. However, non-conventional machining processes such as abrasive jet machining [9], electrochemical machining [10], reactive ion etching [11], lithographie (lithography), galvanoformung (electroforming) and abformung (molding) (LIGA) [12], electrical discharge machining [13], and laser surface texturing [14] have been widely used. Among these, laser surface texturing (LST) provides greater advantages over the other processes. In LST, the controlled texture dimensions are achieved in shorter processing time without affecting the environment [15].

Siripuram and Stephens [16] investigated the influence of standard texture shapes: square, circle, diamond, hexagonal, and triangular, on the performance of hydrodynamic lubrication using the Reynolds boundary condition. At a constant texture height, the friction coefficient is found to be least affected by texture shape and largely affected by texture density. Marian et al. [17] considered a simplified cavitation model for a square textured thrust bearing. They found that the square texture has the potential to improve the hydrodynamic characteristics. Yu et al. [18] found that under cavitation conditions, the square texture performs better than the circular texture in minimizing friction. Under the cavitation effect, Nanbu et al. [19] analyzed the influence of wedge-shaped texture bottom profiles on hydrodynamic characteristics. They found that the textured bottom profile strongly influences the pressure distribution and film thickness. Shen and Khonsari [20] observed that cavitation occurs in the divergent region of the texture, which leads to an asymmetric distribution of pressure. Under this mechanism, the load capacity generated by a rectangular bottom profile is larger than for triangular (oblique and isosceles) bottom profiles. Without a cavitation effect, Han et al. [21] found that the divergence and convergence clearance in a symmetrical texture bottom profile are balanced. However, an asymmetrical bottom profile exhibited greater potential to enhance hydrodynamic characteristics. Similarly, Schuh and Ewoldt [22] found that an asymmetric bottom profile generates a normal force and reduces the shear stress and friction coefficient. Furthermore, Lee et al. [23] noted a significant improvement in hydrodynamic performance with an arbitrarily shaped texture bottom profile.

The influence of the texture shape on hydrodynamic performance can be effectively and qualitatively analyzed using design and optimization. Fesanghary and Khonsari [24] maximized the load capacity of a sectorial-shaped thrust bearing by adopting a

quadrilateral-shaped film profile using the sequential quadratic programming (SQP) optimization technique. Shen and Khonsari [25] presented the numerical optimization of the texture top profile using SQP for maximization of the load capacity. Under unidirectional and bidirectional sliding, the optimum texture profiles obtained were chevron-type and trapezoid-like, respectively. Lin et al. [26] optimized an arbitrary texture bottom profile using sequential linear programming (SQL) to increase the normal force and decrease the friction force. In contrast, Zhang et al. [27] optimized an irregular texture shape to minimize the friction coefficient and maximize the load capacity using a genetic algorithm (GA) optimization technique. For this analysis, texture size and depth were assumed to be constant. Wang et al. [28] used the hybrid GA–SQP optimization technique to evaluate a grooved bottom profile. The optimized profile showed better load capacity than common profiles such as the micro wedge and step profiles. Moreover, they presented the numerical optimization of a chevron-shaped grooved texture to maximize the load capacity of a thrust bearing using the hybrid GA–SQP technique [29]. They experimentally confirmed that the optimum chevron-shaped grooved texture reduces the friction coefficient and the temperature rise of a specimen. Rahmani et al. [30, 31] optimized various standard texture profiles: square, rectangle, and isosceles triangle, using an analytical approach for maximization of the load capacity and minimization of the friction coefficient. Chen et al. [32] applied the Taguchi L27 design method to maximize the load capacity and minimize the fluid leakage of an asymmetrical herringbone groove for a miniature hydrodynamic journal bearing. Shinde and Pawar [33] applied a Taguchi-based grey relational analysis multi-objective optimization technique to a grooved texture journal bearing. They found that groove parameters such as groove location, width, height, spacing between grooves, and number of grooves affect the bearing's performance. Overall, the optimization technique has been proven effective for investigating the influence of process parameters on hydrodynamic performance.

From the above research, it is observed that considerable work on different texture bottom profiles has been carried out. In addition, several authors have presented the optimization of texture geometry to investigate the hydrodynamic performance and have found that the texture bottom profiles influence the hydrodynamic performance along with specific process parameters. However, to the best of the authors' knowledge, a comparative analysis of commonly used texture bottom profiles such as flat, triangular, and curved using multi-objective optimization of variable process parameters (texture density, aspect ratio, and flow speed), has not been reported. Thus, in the present work, a square texture with different bottom profiles such as flat, triangle T1, triangle T2, and curved, are analyzed under unidirectional sliding with the Reynolds cavitation boundary condition.

The analysis of the variable process parameters: aspect ratio, texture density, and flow speed, is performed using the response surface methodology-based central composite design (CCD). This is followed by multi-objective optimization using the grey relational analysis (GRA). The optimized solutions of the bottom profiles are compared to each other regarding maximization of the load capacity and minimization of the friction coefficient. Additionally, the most significant process parameter for each bottom profile is evaluated.

2 Numerical model

2.1 Governing equations

A textured parallel slider, as shown in Fig. 1(a), is considered. Detailed analysis is performed on a single texture of this surface. A single texture is formed using an imaginary unit cell. The present approach reduces

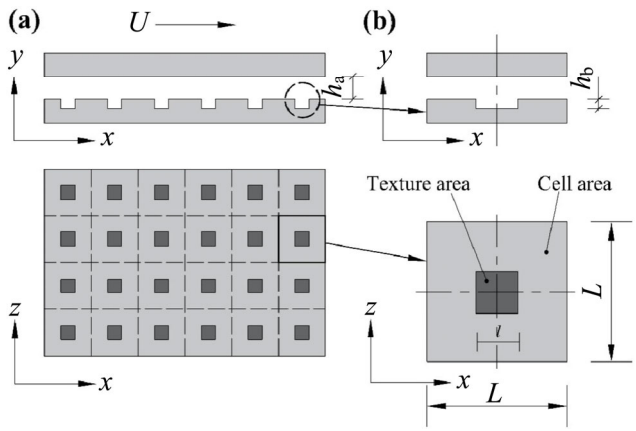

Fig. 1 Texture design of (a) textured parallel slider and (b) square textured unit cell.

the computation time and is relatively easier to model [16]. The texture shape is positioned at the center of a unit cell. A typical texture and unit cell is shown in Fig. 1(b).

It is assumed that the fluid is Newtonian and incompressible. Flow is considered as laminar and steady. The film thickness is so small that the pressure gradient along the film thickness is considered to be zero. Neglecting temperature, inertia, and squeeze film effects, the Reynolds equation can be written as

$$\frac{\partial}{\partial x}\left(h^3\frac{\partial p}{\partial x}\right)+\frac{\partial}{\partial z}\left(h^3\frac{\partial p}{\partial z}\right)=6\mu U\frac{\partial h}{\partial x} \tag{1}$$

The film thickness relationship is given as follows:

$$h(x,z)=\begin{cases}h_a+h_b & (\text{In the texture})\\ h_a & (\text{Elsewhere})\end{cases} \tag{2}$$

where h_a and h_b are the radial clearance and texture depth, respectively.

To solve the Reynolds equation (Eq. (1)), the following boundary conditions are considered for the textured unit cell [16].

Periodic boundary condition:

$$\frac{\partial p}{\partial x}\left(-\frac{L}{2},z\right)=\frac{\partial p}{\partial x}\left(\frac{L}{2},z\right) \tag{3}$$

Atmospheric boundary condition:

$$p\left(x,-\frac{L}{2}\right)=p\left(x,\frac{L}{2}\right)=p_a \tag{4}$$

The Reynolds boundary conditions are applied as cavitation boundaries, as shown below

$$p=p_{cav}=0 \quad \text{and} \quad \frac{\partial p}{\partial x}=0 \quad (p<0)$$

Considering these boundary conditions, the load capacity can be evaluated as

$$W=\int_{-L/2}^{L/2}\int_{-L/2}^{L/2}p(x,z)\mathrm{d}x\mathrm{d}z \tag{5}$$

The above double integration is first solved along the x-direction and then in the z-direction using Simpson's 1/3 integration technique as follows,

$$W_{x_j}=\int_{-L/2}^{L/2}p(x)\mathrm{d}x \tag{6}$$

$$W_{x_j}=\frac{\Delta x}{3}[p_{i=1}+4\,(p_{i=2}+p_{i=4}+\ldots+p_{i=s-2})+2\,(p_{i=3}+p_{i=5}+\ldots+p_{i=s-1})+p_s] \tag{7}$$

$$W=\int_{-L/2}^{L/2}W_{x_j}\mathrm{d}z \tag{8}$$

$$W=\frac{\Delta z}{3}\left[W_{x_{j=1}}+4\left(W_{x_{j=2}}+W_{x_{j=4}}+\ldots+W_{x_{j=s-2}}\right)+2\left(W_{x_{j=3}}+W_{x_{j=5}}+\ldots+W_{x_{j=s-1}}\right)+W_{x_{j=s}}\right] \tag{9}$$

In the above equations, s represents the node of an element. Δx and Δz are the step sizes in the x and z directions, respectively.

Similarly, the friction force can be evaluated as

$$F=\int_{-L/2}^{L/2}\int_{-L/2}^{L/2}\tau(x,z)\mathrm{d}x\mathrm{d}z \tag{10}$$

In Eq. (10), the shear stress (τ) is expressed as

$$\tau(x,z)=\mu\frac{\partial u}{\partial y}(x,z)$$

From Eqs. (5) and (10), the friction coefficient is evaluated as

$$f=\frac{F}{W} \tag{11}$$

2.2 Texture model

To define the texture geometry, two non-dimensional parameters: texture density and the aspect ratio, are used. Texture density (T_d) is defined as the ratio of the texture area (l^2) and the cell area (L^2), whereas aspect ratio (A_r) is defined as the ratio of the texture depth (h_b) and the characteristic length (l) (Fig. 1). The texture depth, converging and diverging wedge shape, and the volume for fluid accumulation play an important role in the hydrodynamic lubrication. Therefore, the texture bottom profile is designed based on these parameters. The texture bottom profiles, namely flat, triangle T1, triangle T2, and curved, are considered for analysis [19]. The geometry of each bottom profile is shown in Fig. 2.

The film thickness for each bottom profile is expressed as follows:

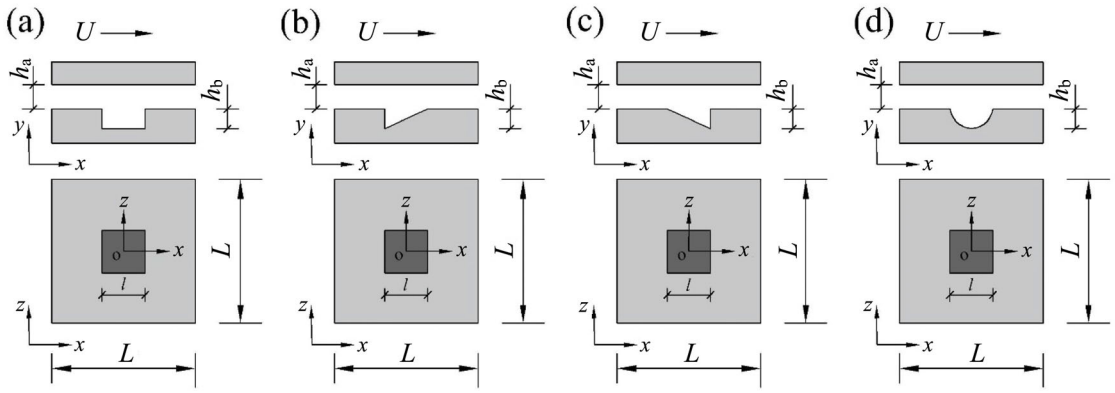

Fig. 2 Texture bottom profiles: (a) flat, (b) triangle T1, (c) triangle T2, and (d) curved.

Flat bottom profile:

$$h(x) = h_a + h_b \tag{12}$$

Triangle T1 bottom profile:

$$h(x) = h_a + h_b - \frac{h_b}{l}x \tag{13}$$

Triangle T2 bottom profile:

$$h(x) = h_a + \frac{h_b}{l}x \tag{14}$$

Curved bottom profile:

$$h(x) = h_a + h_b - r + \sqrt{r^2 - \left(\frac{l}{2} - x\right)^2} \tag{15}$$

In Eq. (15), the radius of the curved texture (r) is expressed as

$$r = \frac{(l/2)^2 + h_a^2}{2h_b}$$

2.3 Computational method and numerical validation

The Reynolds Eq. (1) is discretized using a finite difference method. First order and second order derivatives in the Reynolds equation have been discretized using a first order central difference scheme. A set of simultaneous linear algebraic equations is solved using the Gauss–Seidel iterative technique. The necessary Matlab code was developed and the following convergence criterion was applied.

$$\sum\sum \left| \frac{(p_{i,j})_N - (p_{i,j})_{N-1}}{(p_{i,j})_N} \right| \le 1\times10^{-5} \tag{16}$$

To estimate the suitable step size (number of elements), a grid convergence study was carried out. The grid size was varied from 10 × 10 (= 100 nodes/unit cell) up to 50 × 50 (= 2,500 nodes/unit cell). For each grid size, the friction coefficient is evaluated, as shown in Fig. 3. Based on the accuracy and computing time, a grid size of 25 × 25 (= 625 nodes/unit cell) was used for the simulations. The grid size error is less than 0.5% compared with the grid size of 50 × 50 (= 2,500 nodes/unit cell).

For a square textured parallel slider, the friction coefficients at different texture densities are obtained. The results are validated with Siripuram and Stephens' method [16], as shown in Fig. 4, which indicated good agreement.

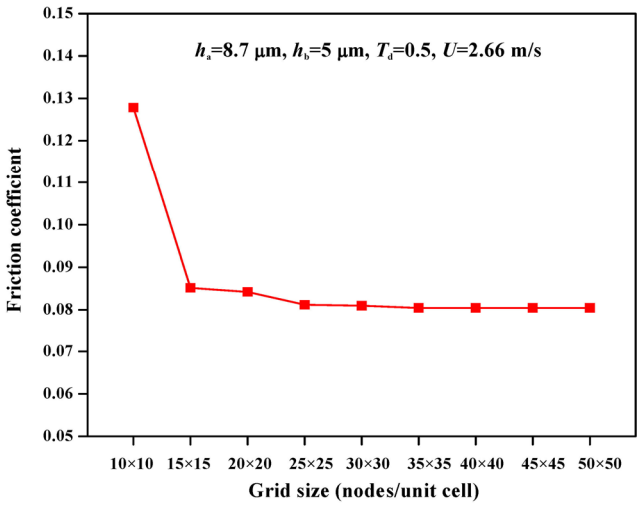

Fig. 3 Effect of grid size on friction coefficient.

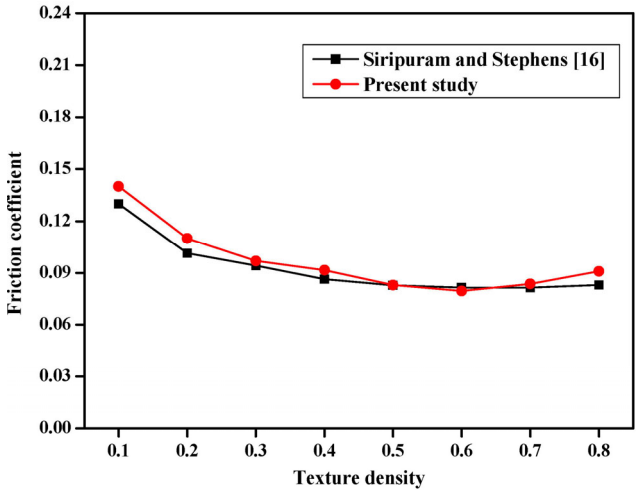

Fig. 4 Friction coefficient of square textured unit cell.

3 Design and optimization

3.1 Design of experiment using response surface methodology

The process parameters of the parallel slider are radial clearance, flow speed, fluid film viscosity, and fluid film temperature. However, the process parameters of the surface texture (texture density and aspect ratio) are non-dimensional parameters. The present study focused on investigating the influence of optimized texture bottom profiles on hydrodynamic characteristics. Therefore, the radial clearance, fluid film viscosity, and fluid film temperature are considered as fixed parameters [33], whereas the aspect ratio, texture density, and flow speed are considered to be variable process parameters [14]. The developed model for the fixed and variable process parameters is shown in Fig. 5.

To investigate the influence of each variable process parameter qualitatively, the proper range is selected. Texture density is varied in the range of 0.4–0.8 [16] and the aspect ratio is varied in the range of 0.005–0.025 [34, 35]. For the flow speed, the range is considered to be 0.66–2.66 m/s, which is commonly used in parallel slider applications [16, 25, 27, 28]. The design and analysis of these variable process parameters is performed using response surface methodology-based CCD. CCD is based on the second order design. It is a five-level design model [36]. The relationship between the indexing of levels and the corresponding numerical values is given below

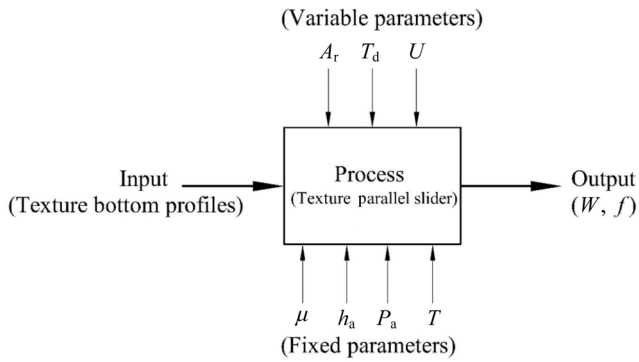

Fig. 5 Model of the process.

$$\text{Aspect ratio: } A = [A_r - (A_{rmax} + A_{rmin})/2]/(A_{rmax} - A_{rmin})/2 \quad (17)$$

$$\text{Texture density: } B = [T_d - (T_{dmax} + T_{dmin})/2]/(T_{dmax} - T_{dmin})/2 \quad (18)$$

$$\text{Flow speed: } C = [U - (U_{max} + U_{min})/2]/(U_{max} - U_{min})/2 \quad (19)$$

In the equations, A, B, and C are the indexed values of the aspect ratio (A_r), texture density (T_d), and flow speed (U), respectively. The subscripts max and min indicate the maximum and minimum values, respectively. The fixed parameters [16] and the values obtained at each level for the variable process parameters are given in Tables 1 and 2, respectively.

For CCD analysis, the number of runs required is given as number of runs,

$$N = 2^a + 2a + b \quad (20)$$

where, a is the number of variable process parameters (a = 3) and b indicates the number of center points (b = 6).

Solving Eq. (20), a total of 20 runs is obtained. For each run, the combination of variable process parameters is obtained using Design-Expert 9.0.1, and these are shown in Table 3. The hydrodynamic

Table 1 Fixed parameters for the analysis.

Parameter	Symbol	Value	Unit
Fluid viscosity	μ	0.042	Pa·s
Radial clearance	h_a	8.7	μm
Atmosphere pressure	p_a	1	bar
Fluid temperature	T	20	°C

Table 2 Variable parameters for the analysis.

Parameter	Symbol	Unit	Range	Level				
				1	2	3	4	5
Aspect ratio	A_r	—	0.005–0.025	0.005	0.01	0.015	0.02	0.025
Texture density	T_d	—	0.4–0.8	0.4	0.5	0.6	0.7	0.8
Flow speed	U	m/s	0.66–2.66	0.66	1.16	1.66	2.16	2.66

Table 3 Performance parameters of the texture bottom profiles.

Run No.	Process parameter			Performance characteristic of bottom profiles							
				Flat		Triangle T1		Triangle T2		Curved	
	A_r	T_d	U	W_{Flat}	f_{Flat}	W_{T1}	f_{T1}	W_{T2}	f_{T2}	W_{curved}	f_{curved}
1	0.005	0.6	1.66	0.0667	0.0979	0.0344	0.1900	0.0598	0.1093	0.0560	0.1167
2	0.01	0.5	1.16	0.0652	0.0667	0.0341	0.1273	0.0551	0.0789	0.0532	0.0817
3	0.01	0.7	1.16	0.0624	0.0590	0.0343	0.1071	0.0639	0.0575	0.0546	0.0674
4	0.01	0.5	2.16	0.1214	0.0667	0.0635	0.1273	0.1026	0.0789	0.0990	0.0817
5	0.01	0.7	2.16	0.1161	0.0590	0.0640	0.1071	0.1190	0.0575	0.1017	0.0674
6	0.015	0.6	0.66	0.0407	0.0514	0.0239	0.0876	0.0396	0.0529	0.0348	0.0601
7	0.015	0.4	1.66	0.0930	0.0682	0.0533	0.1189	0.0820	0.0774	0.0754	0.0841
8	0.015	0.6	1.66	0.1025	0.0514	0.0601	0.0876	0.0996	0.0529	0.0876	0.0601
9	0.015	0.6	1.66	0.1025	0.0514	0.0601	0.0876	0.0996	0.0529	0.0876	0.0601
10	0.015	0.6	1.66	0.1025	0.0514	0.0601	0.0876	0.0996	0.0529	0.0876	0.0601
11	0.015	0.6	1.66	0.1025	0.0514	0.0601	0.0876	0.0996	0.0529	0.0876	0.0601
12	0.015	0.6	1.66	0.1025	0.0514	0.0601	0.0876	0.0996	0.0529	0.0876	0.0601
13	0.015	0.6	1.66	0.1025	0.0514	0.0601	0.0876	0.0996	0.0529	0.0876	0.0601
14	0.015	0.8	1.66	0.0746	0.0553	0.0477	0.0864	0.0928	0.0454	0.0727	0.0568
15	0.015	0.6	2.66	0.1642	0.0514	0.0963	0.0876	0.1595	0.0529	0.1404	0.0601
16	0.02	0.5	1.16	0.0636	0.0608	0.0436	0.0887	0.0662	0.0584	0.0596	0.0649
17	0.02	0.7	1.16	0.0650	0.0465	0.0422	0.0716	0.0734	0.0411	0.0588	0.0514
18	0.02	0.5	2.16	0.1184	0.0608	0.0812	0.0887	0.1233	0.0584	0.1109	0.0649
19	0.02	0.7	2.16	0.1210	0.0460	0.0786	0.0710	0.1367	0.0405	0.1095	0.0509
20	0.025	0.6	1.66	0.0848	0.0554	0.0653	0.0719	0.0997	0.0462	0.0839	0.0560

characteristics (load capacity and friction coefficient) for each texture bottom profile are obtained for each combination.

3.2 Multi-objective optimization using GRA

In the present study, the aim is to maximize the load capacity and minimize the friction coefficient. To obtain these output responses, GRA multi-objective optimization technique is used. It is an effective technique used to optimize variable process parameters. Moreover, the most significant process parameter affecting the output responses is evaluated. To obtain the optimized results, the following steps are applied [33].

Step 1: Normalization

The output responses are normalized in the range of 0–1. To evaluate the levels in GRA, the better larger and better smaller characteristics are used; the load capacity should be high and the friction coefficient should be low. To evaluate this, the original sequence is normalized

as follows:

(a) Load capacity: Larger is better

The normalization equation is given as

$$q_i^*(k) = \frac{q_i(k) - \min[q_i(k)]}{\max[q_i(k)] - \min[q_i(k)]} \quad (21)$$

where $k = 1$ and $i = 1$–20.

(b) Friction coefficient: Smaller is better

The normalization equation is given as

$$q_i^*(k) = \frac{\max[q_i(k)] - q_i(k)}{\max[q_i(k)] - \min[q_i(k)]} \quad (22)$$

where $k = 2$ and $i = 1$–20.

Step 2: Deviation sequence

Deviation sequence $\Delta o_i(k)$ is given as

$$\Delta o_i(k) = \left| q_o^*(k) - q_i^*(k) \right| \quad (23)$$

Step 3: Grey relational coefficient (GRC)

The GRC $\xi_i(k)$ is given as follows:

$$\xi_i(k) = \frac{\Delta_{\min} + \alpha \Delta_{\max}}{\Delta o_i^*(k) + \alpha \Delta_{\max}} \quad (24)$$

In the present analysis, both the load capacity and friction coefficient are considered to be equally important output responses. Thus, an equal weight is assigned to both load capacity and friction coefficient [33, 36]. To assign equal weights, the value of α is 0.5.

Step 4: Grey relational grade (GRG)

The GRG evaluates the overall multi-performance characteristics using the average sum of the grey relational coefficients as follows:

$$\text{GRG} = \frac{1}{n} \sum_{k=1}^{n} \xi_i(k) \quad (25)$$

The flow chart of the grey relational analysis for multi-objective optimization is shown in Fig. 6.

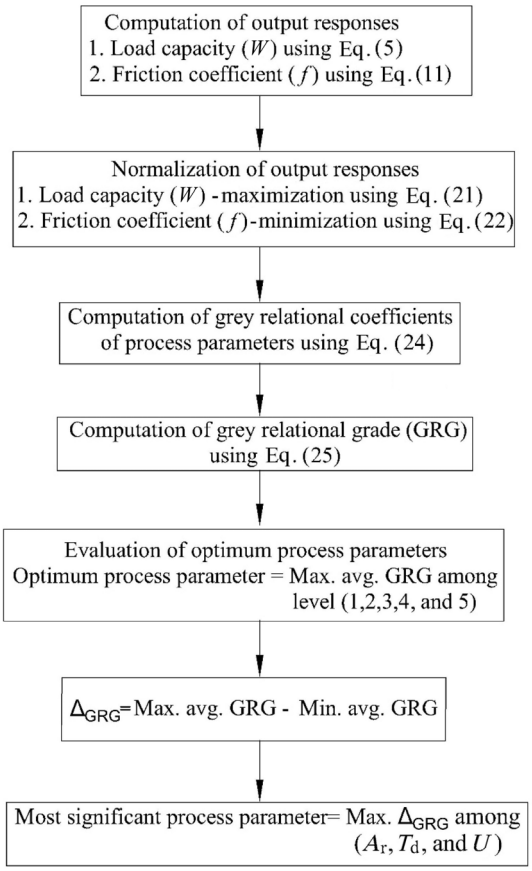

Fig. 6 Flow chart of GRA for multi-objective optimization.

4 Results and discussion

The process parameters: aspect ratio, texture density, and flow speed, are analyzed using the response surface methodology-based CCD. Based on this, the individual effect of these process parameters on hydrodynamic characteristics is investigated. Furthermore, multi-objective optimization of the variable process parameters is performed for each bottom profile using GRA.

4.1 Variable process parameters

The individual effects of process parameters such as aspect ratio, texture density, and flow speed on the load capacity and friction coefficient are described as follows.

4.1.1 Aspect ratio

For the flat bottom profile, upon increasing the aspect ratio, the hydrodynamic characteristics such as load capacity and friction coefficient first improve and then decline, as shown in Figs. 7(a) and 7(b), respectively. However, for asymmetrical bottom profiles (triangle T2 and curved), the load capacity first increases and then remains stable, while the friction coefficient decreases continuously. In contrast, the triangle

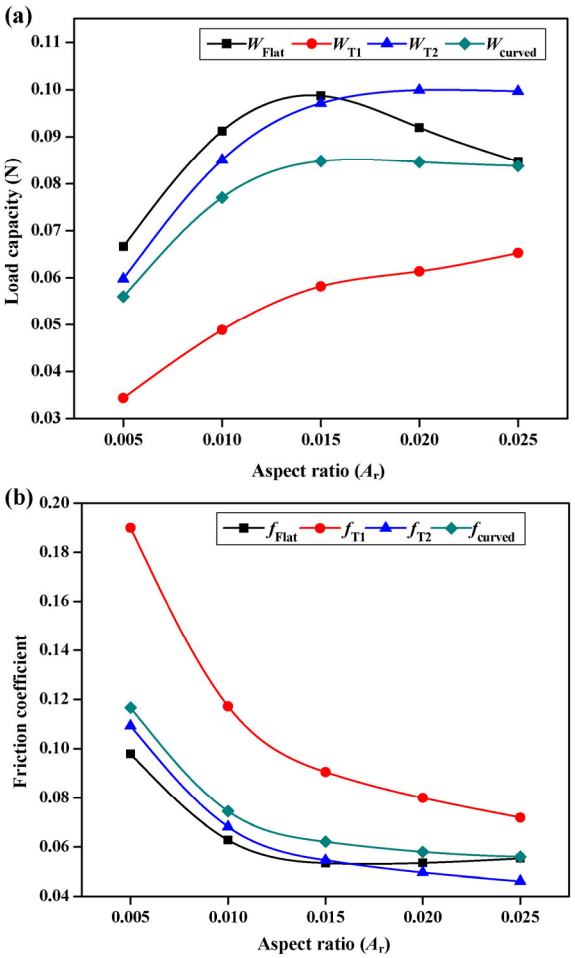

Fig. 7 Effect of aspect ratio on (a) load capacity and (b) friction coefficient.

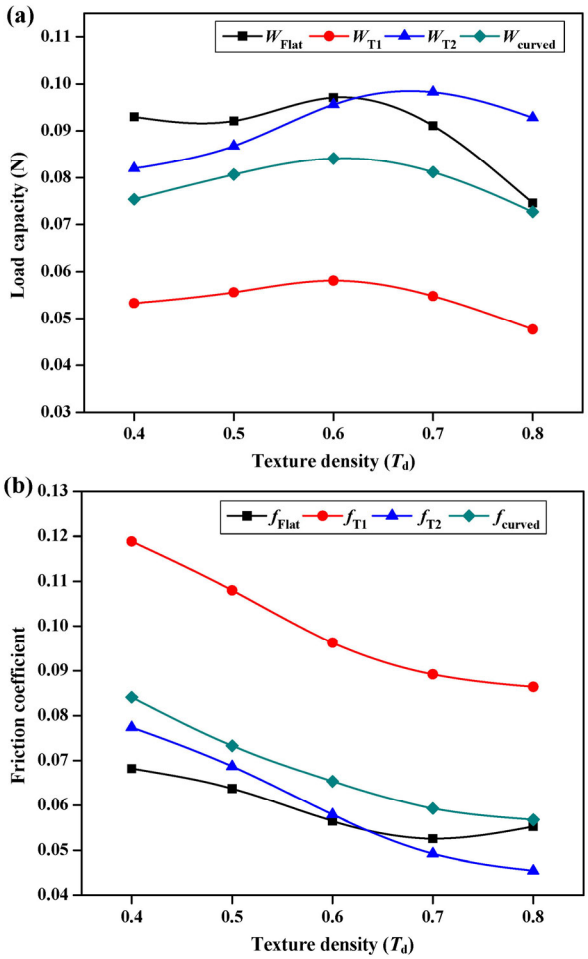

Fig. 8 Effect of texture density on (a) load capacity and (b) friction coefficient.

T1 bottom profile performs the worst regarding both increasing the load capacity and decreasing the friction coefficient.

4.1.2 *Texture density*

For each bottom profile, upon increasing the texture density, the load capacity first increases and then decreases, as shown in Fig. 8(a). The triangle T2 bottom profile exhibits the highest load capacity at a texture density (T_d) of 0.7. The other bottom profiles (flat, triangle T1, and curved) exhibit the highest load capacity at T_d = 0.6. The friction coefficient for each asymmetric bottom profile decreases continuously. The decreasing rate is more pronounced at smaller values of T_d, as shown in Fig. 8(b). Conversely, for a flat bottom profile, the friction coefficient is minimum at T_d = 0.7 and increases at T_d = 0.8. Individually, the triangle T1 bottom profile is found to be the least effective regarding both load capacity and friction coefficient.

4.1.3 *Flow speed*

Upon increasing the flow speed, the load capacity increases, as shown in Fig. 9(a). This is expected and can be predicted from the Reynolds equation. Each texture bottom profile followed the same trend. Flat and triangle T2 bottom profiles achieved almost the same load capacity, followed by curved and triangle T1. However, upon increasing the flow speed, the friction coefficient first increases, remains stable for some time, and later decreases for each bottom profile, as shown in Fig. 9(b). For all process parameters, the triangle T1 and curved bottom profiles were found to be less efficient than flat and triangle T2 profiles regarding increasing the load capacity and decreasing the friction coefficient.

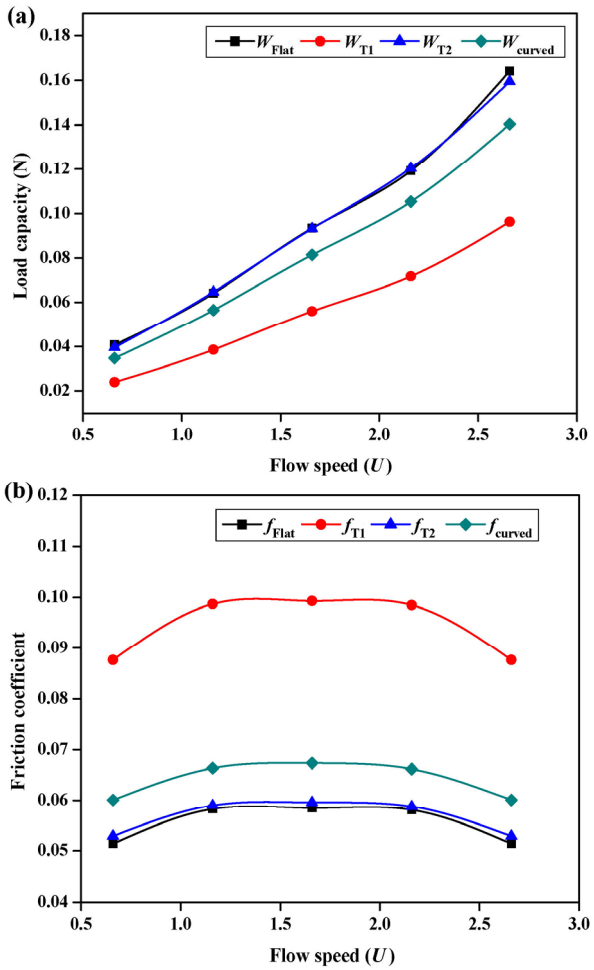

Fig. 9 Effect of flow speed on (a) load capacity and (b) friction coefficient.

4.2 Optimized texture bottom profile

The optimum process parameters of each texture bottom profile are first analyzed and then compared for maximum load capacity and minimum friction coefficient.

4.2.1 Flat bottom profile

As discussed in Section 3.2, GRG is obtained for 20 runs. The GRG measures the combined effect of increasing the load capacity and decreasing the friction coefficient (multi-objective optimization). The highest GRG is termed as rank 1 and the lowest as rank 20, as shown in Table 4. Rank 1 is obtained for run No. 15. Thus, the process parameters corresponding to run No. 15 provide the best solution among the 20 runs, although it may not be the optimum solution.

To estimate the optimum solution, an average GRG is calculated at each level for all process parameters. The maximum average GRG is obtained at level 3 and is used to evaluate the optimum aspect ratio, as shown in Fig. 10(a). For level 3, the corresponding parametric value of the aspect ratio is 0.015 (Table 2). Thus, the optimum aspect ratio for a flat bottom profile is 0.015. For texture density, the maximum average GRG is obtained at level 4, as shown in Fig. 10(b), and the corresponding parametric value of the texture density is 0.7. The maximum average GRG for flow speed is obtained at level 5 (Fig. 10(c)), and from Table 2, the optimum flow speed is found to be 2.66 m/s. For the flat bottom profile, the optimum aspect ratio, texture density, and flow speed are found to be 0.015, 0.7, and 2.66 m/s, respectively. The corresponding optimum texture geometry and the pressure profile are given in Figs. 11(a) and 11(b), respectively. It is observed that pressure is first reduced in the leading region and then generates an additional hydrodynamic effect in the trailing region. Under this optimum condition, the load capacity and friction coefficient are obtained as 0.1565 N and 0.0481, respectively.

The most significant process parameter that serves to improve the hydrodynamic performance is evaluated. For each process parameter, the difference between the maximum and minimum average GRG (Δ_{GRG}) is calculated, as shown in Table 5. Δ_{GRG} is the highest for flow speed and the lowest for texture density. Therefore, the flow speed is the most significant process parameter to increase load capacity and decrease the friction coefficient, followed by the aspect ratio, while texture density is the least significant process parameter.

4.2.2 Triangle T1 bottom profile

For the triangle T1 bottom profile, the GRG is calculated for each run, as shown in Table 6. The optimum solution is then evaluated by calculating the average GRG at each level for all the process parameters.

For both the aspect ratio and flow speed, the maximum average GRG is obtained at level 5, as shown in Figs. 12(a) and 12(c), respectively, while it is obtained at level 4 for the texture density (Fig. 12(b)). For these levels, the optimum aspect ratio, texture density, and flow speed are found to be 0.025, 0.7, and 2.66 m/s, respectively. The optimum texture geometry

Table 4 GRA of flat bottom profile.

Run No.	Process parameter			Normalization		Deviation		GRC		GRG	Rank
	A_r	T_d	U	N_W	N_f	D_W	D_f	GRC_W	GRC_f		
1	0.005	0.6	1.66	0.2108	0.0000	0.7892	1.0000	0.3878	0.3333	0.3606	20
2	0.01	0.5	1.16	0.1983	0.6021	0.8017	0.3979	0.3841	0.5569	0.4705	19
3	0.01	0.7	1.16	0.1754	0.7499	0.8246	0.2501	0.3775	0.6666	0.5220	16
4	0.01	0.5	2.16	0.6533	0.6021	0.3467	0.3979	0.5905	0.5569	0.5737	14
5	0.01	0.7	2.16	0.6108	0.7499	0.3892	0.2501	0.5623	0.6666	0.6144	10
6	0.015	0.6	0.66	0.0000	0.8965	1.0000	0.1035	0.3333	0.8285	0.5809	13
7	0.015	0.4	1.66	0.4235	0.5724	0.5765	0.4276	0.4645	0.5390	0.5017	18
8	0.015	0.6	1.66	0.5002	0.8965	0.4998	0.1035	0.5001	0.8285	0.6643	9
9	0.015	0.6	1.66	0.5002	0.8965	0.4998	0.1035	0.5001	0.8285	0.6643	8
10	0.015	0.6	1.66	0.5002	0.8965	0.4998	0.1035	0.5001	0.8285	0.6643	7
11	0.015	0.6	1.66	0.5002	0.8965	0.4998	0.1035	0.5001	0.8285	0.6643	6
12	0.015	0.6	1.66	0.5002	0.8965	0.4998	0.1035	0.5001	0.8285	0.6643	5
13	0.015	0.6	1.66	0.5002	0.8965	0.4998	0.1035	0.5001	0.8285	0.6643	4
14	0.015	0.8	1.66	0.2748	0.8216	0.7252	0.1784	0.4081	0.7370	0.5726	15
15	**0.015**	**0.6**	**2.66**	**1.0000**	**0.8965**	**0.0000**	**0.1035**	**1.0000**	**0.8285**	**0.9143**	**1**
16	0.02	0.5	1.16	0.1852	0.7144	0.8148	0.2856	0.3803	0.6364	0.5084	17
17	0.02	0.7	1.16	0.1965	0.9904	0.8035	0.0096	0.3836	0.9812	0.6824	3
18	0.02	0.5	2.16	0.6289	0.7144	0.3711	0.2856	0.5740	0.6364	0.6052	11
19	0.02	0.7	2.16	0.6500	1.0000	0.3500	0.0000	0.5883	1.0000	0.7941	2
20	0.025	0.6	1.66	0.3569	0.8191	0.6431	0.1809	0.4374	0.7343	0.5859	12

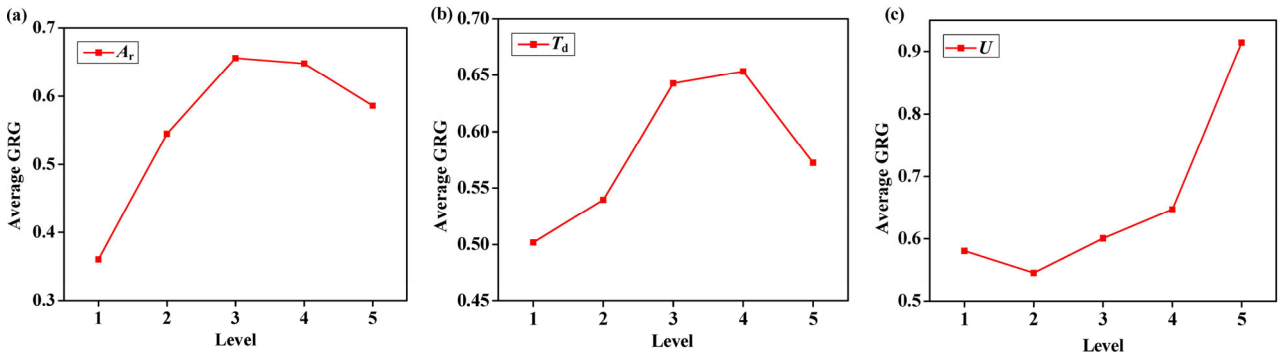

Fig. 10 Influence of flat bottom profile texture design variables (a) aspect ratio, (b) texture density, and (c) flow speed on output responses.

is shown in Fig. 13(a) and the corresponding pressure profile is given in Fig. 13(b). It is found that a large pressure reduction and minimum recovery take place in the leading and trailing region of the triangle T1 texture, respectively. For the optimum process parameters, the load capacity and friction coefficient are determined to be 0.0966 N and 0.0672, respectively.

As discussed in Section 4.2.1, Δ_{GRG} is calculated for each process parameter (Table 7). The highest and lowest Δ_{GRG} are obtained for the aspect ratio and texture density, respectively. Therefore, the aspect ratio is found to be the most significant process parameter, while the texture density is the least significant process parameter.

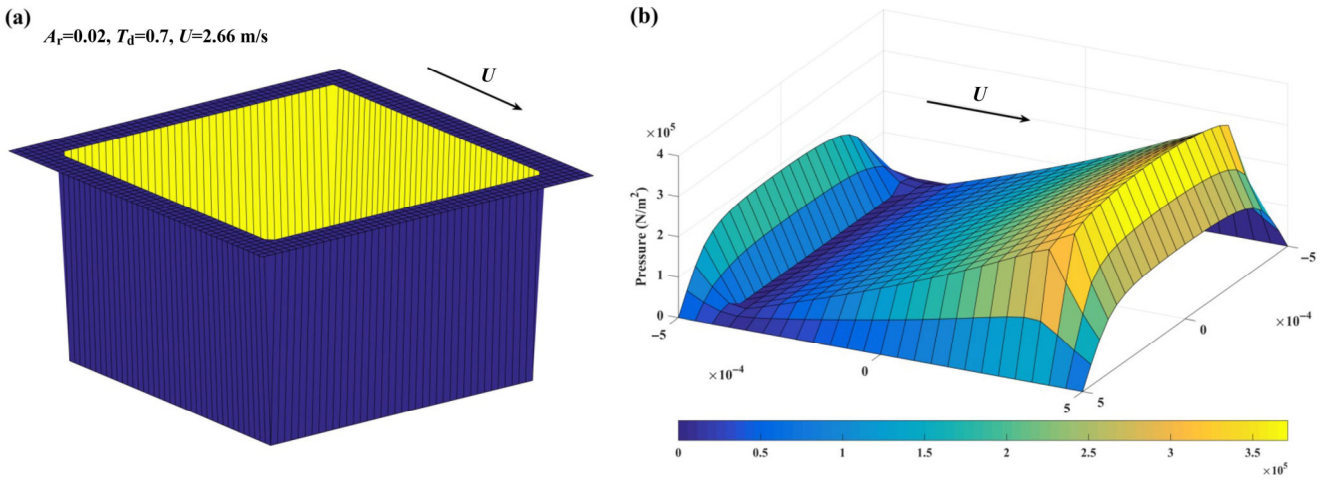

Fig. 11 Optimum (a) texture geometry and (b) pressure profile for flat bottom profile.

Table 5 The most significant process parameter of flat bottom profile.

Process parameter	Symbol	Max. avg. GRG	Min. avg. GRG	Δ_{GRG}	Significant grade
Aspect ratio	A_r	0.6555	0.3606	0.2949	2nd
Texture density	T_d	0.6532	0.5017	0.1515	3rd
Flow speed	U	0.9143	0.5458	0.3685	1st

Table 6 GRA of triangle T1 bottom profile.

Run No.	Process parameter			Normalization		Deviation		GRC		GRG	Rank
	A_r	T_d	U	N_W	N_f	D_W	D_f	GRC_W	GRC_f		
1	0.005	0.6	1.66	0.1447	0.0000	0.8553	1.0000	0.3689	0.3333	0.3511	20
2	0.01	0.5	1.16	0.1413	0.5269	0.8587	0.4731	0.3680	0.5138	0.4409	19
3	0.01	0.7	1.16	0.1442	0.6966	0.8558	0.3034	0.3688	0.6224	0.4956	18
4	0.01	0.5	2.16	0.5476	0.5269	0.4524	0.4731	0.5250	0.5138	0.5194	16
5	0.01	0.7	2.16	0.5532	0.6966	0.4468	0.3034	0.5281	0.6224	0.5752	14
6	0.015	0.6	0.66	0.0000	0.8603	1.0000	0.1397	0.3333	0.7816	0.5575	15
7	0.015	0.4	1.66	0.4065	0.5974	0.5935	0.4026	0.4572	0.5539	0.5056	17
8	0.015	0.6	1.66	0.4997	0.8603	0.5003	0.1397	0.4998	0.7816	0.6407	6
9	0.015	0.6	1.66	0.4997	0.8603	0.5003	0.1397	0.4998	0.7816	0.6407	7
10	0.015	0.6	1.66	0.4997	0.8603	0.5003	0.1397	0.4998	0.7816	0.6407	8
11	0.015	0.6	1.66	0.4997	0.8603	0.5003	0.1397	0.4998	0.7816	0.6407	9
12	0.015	0.6	1.66	0.4997	0.8603	0.5003	0.1397	0.4998	0.7816	0.6407	10
13	0.015	0.6	1.66	0.4997	0.8603	0.5003	0.1397	0.4998	0.7816	0.6407	11
14	0.015	0.8	1.66	0.3291	0.8704	0.6709	0.1296	0.4270	0.7942	0.6106	12
15	**0.015**	**0.6**	**2.66**	**1.0000**	**0.8603**	**0.0000**	**0.1397**	**1.0000**	**0.7816**	**0.8908**	**1**
16	0.02	0.5	1.16	0.2722	0.8516	0.7278	0.1484	0.4072	0.7711	0.5892	13
17	0.02	0.7	1.16	0.2528	0.9951	0.7472	0.0049	0.4009	0.9903	0.6956	5
18	0.02	0.5	2.16	0.7914	0.8516	0.2086	0.1484	0.7057	0.7711	0.7384	4
19	0.02	0.7	2.16	0.7552	1.0000	0.2448	0.0000	0.6714	1.0000	0.8357	2
20	0.025	0.6	1.66	0.5718	0.9923	0.4282	0.0077	0.5387	0.9848	0.7617	3

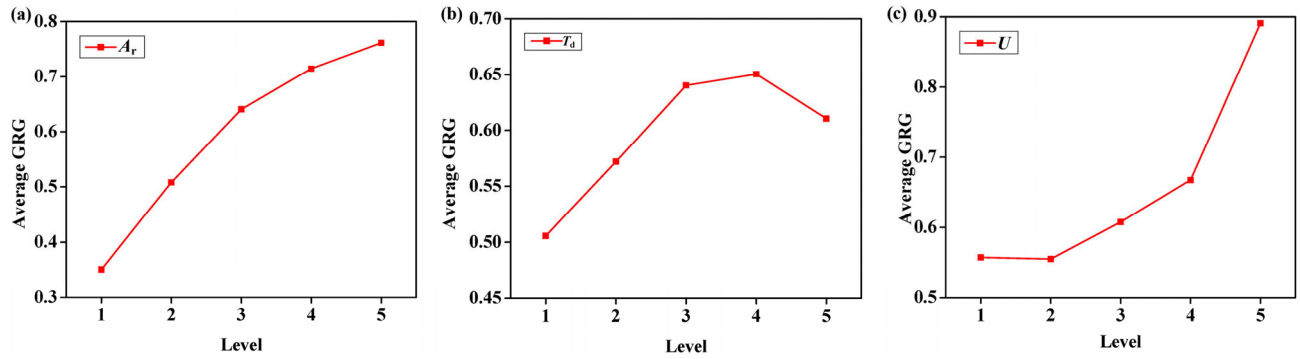

Fig. 12 Influence of triangle T1 bottom profile texture design variables: (a) aspect ratio, (b) texture density, and (c) flow speed on output responses.

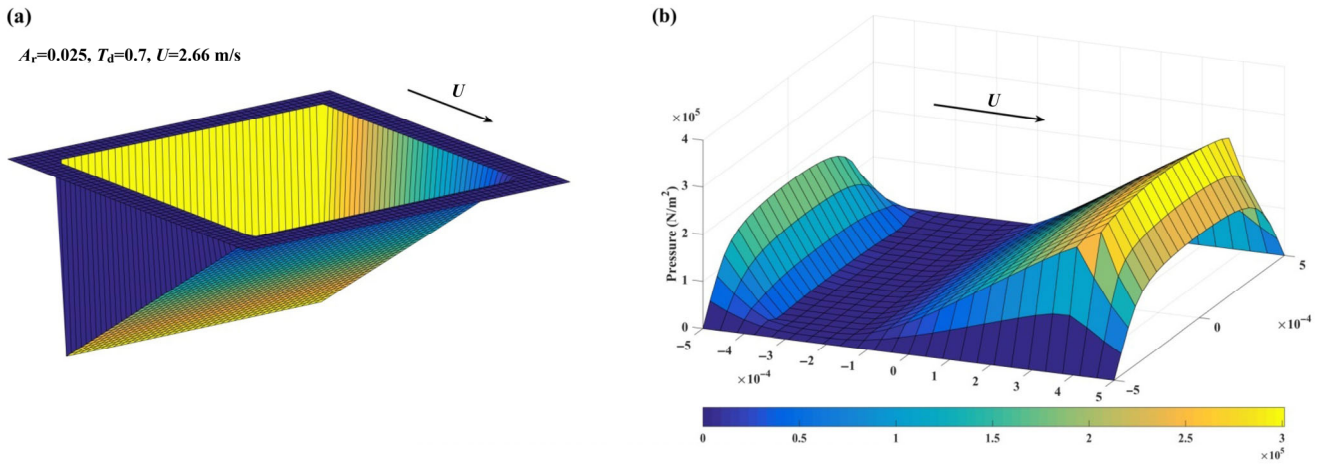

Fig. 13 Optimum (a) texture geometry and (b) pressure profile for triangle T1 bottom profile.

Table 7 The most significant process parameter of triangle T1 bottom profile.

Process parameter	Symbol	Max. avg. GRG	Min. avg. GRG	Δ_{GRG}	Significant grade
Aspect ratio	A_r	0.7617	0.3511	0.4106	1st
Texture density	T_d	0.6505	0.5056	0.1449	3rd
Flow speed	U	0.8908	0.5553	0.3355	2nd

4.2.3 *Triangle T2 bottom profile*

The GRA of the triangle T2 bottom profile is given in Table 8. Similar to Sections 4.2.1 and 4.2.2, the optimum solution of the triangle T2 bottom profile is evaluated.

For the aspect ratio, the maximum average GRG is obtained at level 4, as shown in Fig. 14(a). A similar trend is followed by the texture density, where the maximum average GRG is also obtained at level 4 (Fig. 14(b)). However, upon increasing the flow speed, the hydrodynamic performance improves, but the maximum enhancement (max. avg. GRG) is obtained at level 5 instead of level 4, as shown in Fig. 14(c). Using Table 2, the optimum aspect ratio, texture density, and flow speed are obtained as 0.02, 0.7, and 2.66 m/s, respectively. The optimum texture geometry and pressure profile are shown in Figs. 15(a) and 15(b), respectively. In contrast to the triangle T1 profile, the triangle T2 bottom profile exhibits the least reduction and the highest generation of pressure. This occurs because of the smallest and the largest wedge effects present in the leading and trailing regions, respectively. For the optimum process parameters, the load capacity and friction coefficient are obtained as 0.1684 N and 0.0411, respectively.

Table 8 GRA of triangle T2 bottom profile.

Run No.	Process parameter			Normalization		Deviation		GRC		GRG	Rank
	A_r	T_d	U	N_W	N_f	D_W	D_f	GRC$_W$	GRC$_f$		
1	0.005	0.6	1.66	0.1684	0.0000	0.8316	1.0000	0.3755	0.3333	0.3544	20
2	0.01	0.5	1.16	0.1291	0.4420	0.8709	0.5580	0.3647	0.4726	0.4187	19
3	0.01	0.7	1.16	0.2029	0.7524	0.7971	0.2476	0.3855	0.6688	0.5271	15
4	0.01	0.5	2.16	0.5250	0.4420	0.4750	0.5580	0.5128	0.4726	0.4927	17
5	0.01	0.7	2.16	0.6626	0.7524	0.3374	0.2476	0.5971	0.6688	0.6329	7
6	0.015	0.6	0.66	0.0000	0.8202	1.0000	0.1798	0.3333	0.7355	0.5344	14
7	0.015	0.4	1.66	0.3532	0.4639	0.6468	0.5361	0.4360	0.4826	0.4593	18
8	0.015	0.6	1.66	0.5001	0.8202	0.4999	0.1798	0.5001	0.7355	0.6178	8
9	0.015	0.6	1.66	0.5001	0.8202	0.4999	0.1798	0.5001	0.7355	0.6178	9
10	0.015	0.6	1.66	0.5001	0.8202	0.4999	0.1798	0.5001	0.7355	0.6178	10
11	0.015	0.6	1.66	0.5001	0.8202	0.4999	0.1798	0.5001	0.7355	0.6178	11
12	0.015	0.6	1.66	0.5001	0.8202	0.4999	0.1798	0.5001	0.7355	0.6178	12
13	0.015	0.6	1.66	0.5001	0.8202	0.4999	0.1798	0.5001	0.7355	0.6178	13
14	0.015	0.8	1.66	0.4440	0.9288	0.5560	0.0712	0.4735	0.8753	0.6744	4
15	**0.015**	**0.6**	**2.66**	**1.0000**	**0.8202**	**0.0000**	**0.1798**	**1.0000**	**0.7355**	**0.8677**	**1**
16	0.02	0.5	1.16	0.2219	0.7398	0.7781	0.2602	0.3912	0.6577	0.5245	16
17	0.02	0.7	1.16	0.2822	0.9907	0.7178	0.0093	0.4106	0.9817	0.6961	3
18	0.02	0.5	2.16	0.6979	0.7398	0.3021	0.2602	0.6234	0.6577	0.6406	6
19	0.02	0.7	2.16	0.8101	1.0000	0.1899	0.0000	0.7248	1.0000	0.8624	2
20	0.025	0.6	1.66	0.5013	0.9173	0.4987	0.0827	0.5006	0.8581	0.6793	5

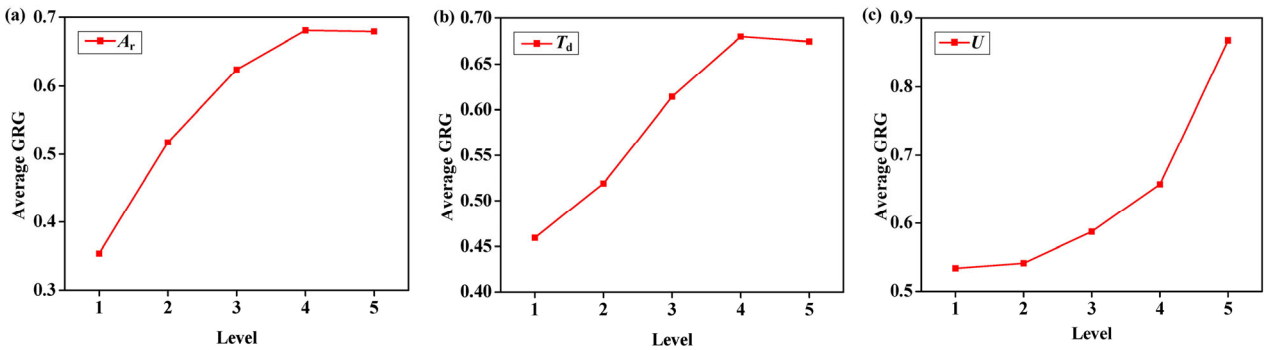

Fig. 14 Influence of triangle T2 bottom profile texture design variables: (a) aspect ratio, (b) texture density, and (c) flow speed on output responses.

From Table 9, the flow speed is found to be the most significant process parameter, followed by the aspect ratio. Texture density is the least significant process parameter regarding the improvement of hydrodynamic performance.

4.2.4 *Curved bottom profile*

For the curved bottom profile, GRA is given in Table 10. Similar to the other bottom profiles, rank 1 is obtained for run No. 15. For this run, the maximum GRG is 0.8910. To investigate the optimum process parameters, the maximum average GRG is calculated for all the process parameters.

For both the aspect ratio and texture density, the maximum average GRG is obtained at level 4, as shown in Figs. 16(a) and 16(b), respectively. The hydrodynamic

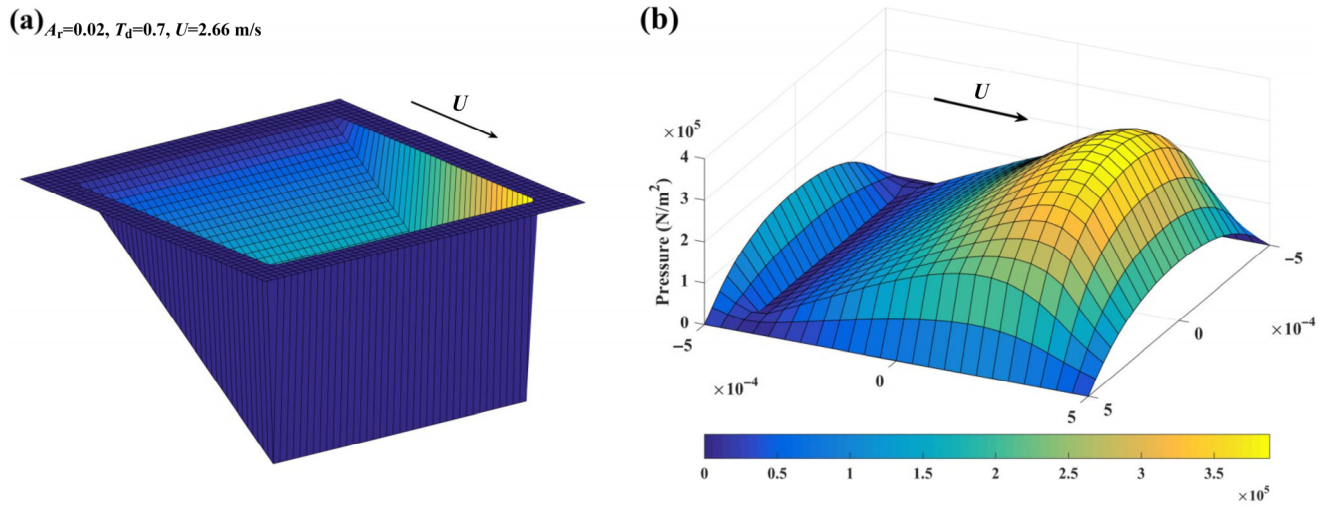

Fig. 15 Optimum (a) texture geometry and (b) pressure profile for triangle T2 bottom profile.

Table 9 The most significant process parameter of triangle T2 bottom profile.

Process parameter	Symbol	Max. avg. GRG	Min. avg. GRG	Δ_{GRG}	Significant grade
Aspect ratio	A_r	0.6809	0.3544	0.3265	2nd
Texture density	T_d	0.6797	0.4593	0.2204	3rd
Flow speed	U	0.8677	0.5344	0.3333	1st

Table 10 GRA of curved bottom profile.

Run No.	Process parameter			Normalization		Deviation		GRC		GRG	Rank
	A_r	T_d	U	N_W	N_f	D_W	D_f	GRC_W	GRC_f		
1	0.005	0.6	1.66	0.2005	0.0000	0.7995	1.0000	0.3848	0.3333	0.3591	20
2	0.01	0.5	1.16	0.1741	0.5321	0.8259	0.4679	0.3771	0.5166	0.4468	19
3	0.01	0.7	1.16	0.1875	0.7497	0.8125	0.2503	0.3810	0.6664	0.5237	17
4	0.01	0.5	2.16	0.6083	0.5321	0.3917	0.4679	0.5607	0.5166	0.5386	16
5	0.01	0.7	2.16	0.6332	0.7497	0.3668	0.2503	0.5769	0.6664	0.6216	13
6	0.015	0.6	0.66	0.0000	0.8606	1.0000	0.1394	0.3333	0.7819	0.5576	14
7	0.015	0.4	1.66	0.3845	0.4954	0.6155	0.5046	0.4482	0.4977	0.4730	18
8	0.015	0.6	1.66	0.5003	0.8606	0.4997	0.1394	0.5001	0.7819	0.6410	7
9	0.015	0.6	1.66	0.5003	0.8606	0.4997	0.1394	0.5001	0.7819	0.6410	8
10	0.015	0.6	1.66	0.5003	0.8606	0.4997	0.1394	0.5001	0.7819	0.6410	9
11	0.015	0.6	1.66	0.5003	0.8606	0.4997	0.1394	0.5001	0.7819	0.6410	10
12	0.015	0.6	1.66	0.5003	0.8606	0.4997	0.1394	0.5001	0.7819	0.6410	11
13	0.015	0.6	1.66	0.5003	0.8606	0.4997	0.1394	0.5001	0.7819	0.6410	12
14	0.015	0.8	1.66	0.3584	0.9107	0.6416	0.0893	0.4380	0.8485	0.6433	6
15	**0.015**	**0.6**	**2.66**	**1.0000**	**0.8606**	**0.0000**	**0.1394**	**1.0000**	**0.7819**	**0.8910**	**1**
16	0.02	0.5	1.16	0.2345	0.7871	0.7655	0.2129	0.3951	0.7013	0.5482	15
17	0.02	0.7	1.16	0.2273	0.9928	0.7727	0.0072	0.3929	0.9858	0.6893	3
18	0.02	0.5	2.16	0.7208	0.7871	0.2792	0.2129	0.6417	0.7013	0.6715	5
19	0.02	0.7	2.16	0.7073	1.0000	0.2927	0.0000	0.6308	1.0000	0.8154	2
20	0.025	0.6	1.66	0.4647	0.9226	0.5353	0.0774	0.4830	0.8660	0.6745	4

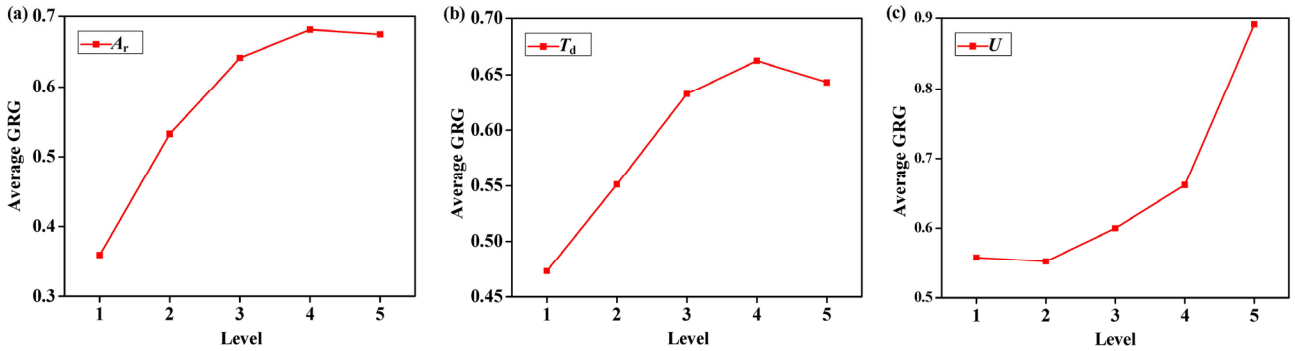

Fig. 16 Influence of curved bottom profile texture design variables (a) aspect ratio, (b) texture density, and (c) flow speed on output responses.

performance first increases up to level 4 and then decreases. For the flow speed, similar to the other bottom profiles, the maximum average GRG is obtained at level 5 (Fig. 16(c)). The corresponding aspect ratio, texture density, and flow speed are 0.02, 0.7, and 2.66 m/s, respectively. For these process parameters, the optimum texture geometry and pressure profile are shown in Figs. 17(a) and 17(b), respectively. For the curved bottom profile, the gentle variation in texture depth results in higher pressure generation than the triangle T1 can produce but is less than the triangle T2 and flat bottom profiles. The hydrodynamic characteristics (the load capacity and friction coefficient) produced by the optimum process parameters are 0.1348 N and 0.0514, respectively.

For the curved bottom profile, the flow speed and texture density are found to be the most significant and the least significant process parameters, respectively (Table 11).

4.3 Comparative analysis

The set of optimum process parameters and the corresponding output responses are summarized in Table 12 for each bottom profile. The triangle T2 bottom

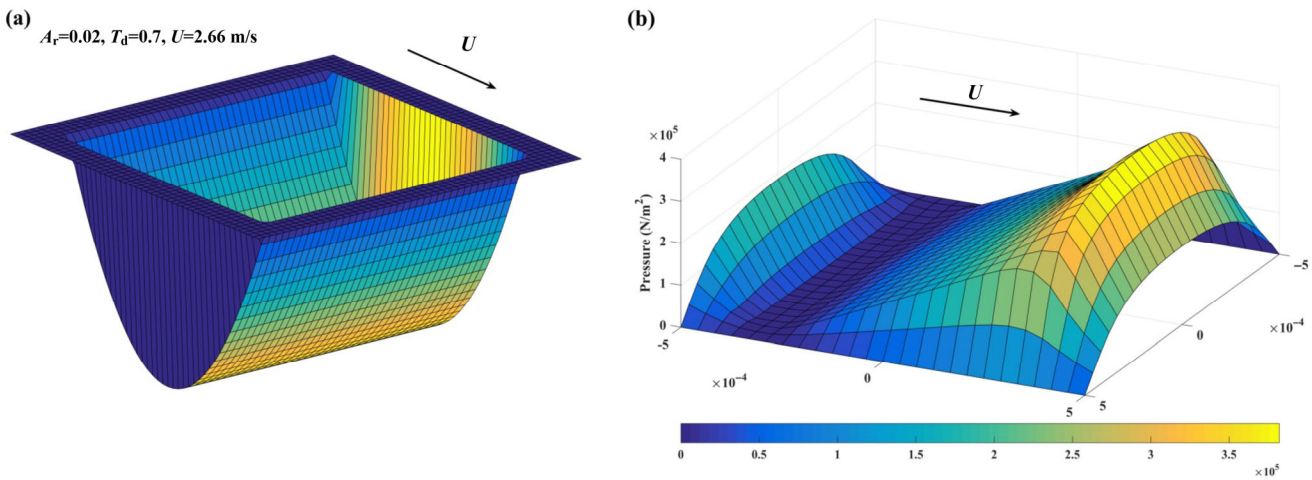

Fig. 17 Optimum (a) texture geometry and (b) pressure profile for curved bottom profile.

Table 11 The most significant process parameter of curved bottom profile.

Process parameters	Symbol	Max. avg. GRG	Min. avg. GRG	Δ_{GRG}	Significant grade
Aspect ratio	A_r	0.6811	0.3591	0.3220	2nd
Texture density	T_d	0.6625	0.4730	0.1895	3rd
Flow speed	U	0.8910	0.5520	0.3390	1st

Table 12 Comparative analysis of optimized bottom profile textures.

Texture bottom profile	Optimum process parameter			Output response		Relative output response	
	T_d	A_r	U	W	f	$W_{relative}$	$f_{relative}$
Flat	0.7	0.015	2.66	0.1565	0.0481	–7.07%	+17.03%
Triangle T1	0.7	0.025	2.66	0.0966	0.0672	–42.64%	+63.5%
TriangleT2	0.7	0.02	2.66	0.1684	0.0411	0	0
Curved	0.7	0.02	2.66	0.1348	0.0514	–19.95%	+25.06%

profile achieves the highest load capacity and the lowest friction coefficient compared to the flat, triangle T1, and curved bottom profiles, where the triangle T1 bottom profile achieves the lowest load capacity and the highest friction coefficient (the worst results). The triangle T1 profile has 42.61% reduced load capacity and 63.5% greater friction coefficient than the triangle T2 bottom profile. This implies that the type of texture bottom profile influences the hydrodynamic performance significantly.

For each optimized bottom profile, the hydrodynamic pressure decreases in the leading region, while additional hydrodynamic pressure is generated by the wedge/step effect in the trailing region, as shown in Figs. 11(b), 13(b), 15(b), and 17(b). The higher pressure further separates the surfaces [37] and improves the load capacity [38], resulting in lower local shear stress [39] and a lower friction coefficient [22, 40]. Flat, triangle T2, and curved bottom profiles produce very similar values of local maximum pressure at the trailing edge; however, the triangle T2 bottom profile induces the highest average hydrodynamic pressure, as it produces the largest wedge effect in the direction of flow from the leading to trailing edge. This causes the greatest separation between surfaces and provides the maximum improvement in load capacity and reduction in shear stress, and hence produces the lowest friction coefficient. Both flat and triangle T2 bottom profiles have a larger step at the trailing edge (Fig. 2), but the flat bottom profile has constant depth in the leading region, which leads to a greater decrease and lower recovery of pressure than the triangle T2. In comparison with the triangle T2, the triangle T1 bottom profile has maximum and minimum wedges at the leading and trailing regions, respectively. This results in larger pressure reduction in the leading zone, as shown in Fig. 13(b). A minimal hydrodynamic pressure is generated in the trailing region, and thus leads to the least separation between surfaces. This results in the lowest load capacity and the highest friction coefficient. In contrast, for a curved bottom profile, the texture depth varies gently. Therefore, the pressure reduction in the leading region is lower and pressure generation in the trailing region is higher than for the triangle T1 profile, but generates lower pressure in the trailing end than the flat and triangle T2 bottom profiles.

4.4 Regression model tests

A regression model was developed using Design Expert 9.0.1 to determine the relationships between the variable process parameters and the output responses. Conformity of the optimized results is based on a flat bottom profile. The predicted second order regression equation for the load capacity and friction coefficient is as follows,

$$W = -0.2131 + 8.4666 \times A_r + 0.5307 \times T_d + 0.0585 \times U - 265.9286 \times A_r^2 - 0.4636 \times T_d^2 \quad (26)$$

$$f = 0.2433 - 8.9227 \times A_r - 0.3363 \times T_d + 246.4643 \times A_r^2 + 0.2437 \times T_d^2 \quad (27)$$

The load capacity and friction coefficient for the 20 runs were calculated using numerical simulations, and the predicted regression model results are shown in Figs. 18(a) and 18(b), respectively. The results obtained using the regression model show good agreement with the numerical simulated results. The deviation between the two is within 4% for both load capacity and friction coefficient. This deviation occurred because of residuals in the regression model.

Moreover, the deviation between the numerical and regression model results for optimized process parameters is less than 2% (Table 13).

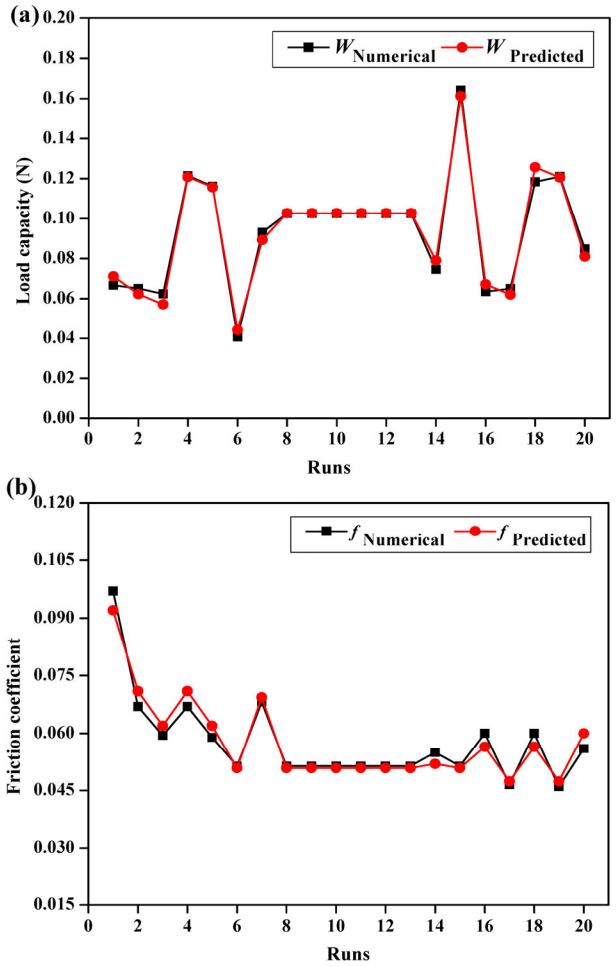

Fig. 18 Numerical and regression model results for (a) load capacity and (b) friction coefficient.

Table 13 Numerical and predicted regression model results.

Optimized process parameter			Numerical result		Predicted regression model result		Error (%)	
T_d	A_r	U	W	f	W	f	W	f
0.7	0.015	2.66	0.1565	0.0481	0.1541	0.0490	1.53	1.87

5 Conclusions

In the present work, various texture bottom profiles: flat, triangle T1, triangle T2, and curved, are analyzed using response surface methodology-based CCD. This is followed by GRA multi-objective optimization. The aspect ratio, texture density, and flow speed are considered as variable process parameters for the maximization of the load capacity and the minimization of the friction coefficient. For the optimized process parameters of each bottom profile, the output responses are compared with each other. It is concluded that:

(1) The optimum aspect ratio is found in the range of 0.02–0.025. The optimum texture density and flow speed are found to be 0.7 and 2.66 m/s, respectively.

(2) In comparison with other bottom profiles, the triangle T2 profile produced the highest load capacity and the lowest friction coefficient. In contrast, the triangle T1 bottom profile produced the lowest load capacity and the highest friction coefficient.

(3) For the triangle T2 bottom profile, to maximize the load capacity and to minimize the friction coefficient, the flow speed was found to be the most significant process parameter, followed by the aspect ratio. Texture density was found to be the least significant parameter among the three parameters considered.

(4) The results using the predicted regression model with optimum texture process parameters deviate by less than 2% from numerical results.

References

[1] Etsion I. Modeling of surface texturing in hydrodynamic lubrication. *Friction* **1**(3): 195–209 (2013)

[2] Gropper D, Wang L, Harvey T J. Hydrodynamic lubrication of textured surfaces: A review of modeling techniques and key findings. *Tribol Int* **94**: 509–529 (2016)

[3] Kligerman Y, Etsion I. Analysis of the hydrodynamic effects in a surface textured circumferential gas seal. *Tribol Trans* **44**(3): 472–478 (2001)

[4] Kligerman Y, Etsion I, Shinkarenko A. Improving tribological performance of piston rings by partial surface texturing. *J Tribol* **127**(3): 632–638 (2005)

[5] Yagi S, Katayama N, Hasegawa H, Matsushita H, Okihara S. Effects of microscale texture on the tribological behavior of paper-based friction materials for a wet clutch. *Tribol Online* **10**(5): 390–396 (2015)

[6] Jesudass Thomas S, Kalaichelvan K. Comparative study of the effect of surface texturing on cutting tool in dry cutting. *Mater Manuf Process* **33**(6): 683–694 (2018)

[7] Ghosh S, Abanteriba S. Status of surface modification techniques for artificial hip implants. *Sci Technol Adv Mater* **17**(1): 715–735 (2016)

[8] Arslan A, Masjuki H H, Kalam M A, Varman M, Mufti R A, Mosarof M H, Khuong L S, Quazi M M. Surface texture manufacturing techniques and tribological effect of surface texturing on cutting tool performance: A review. *Crit Rev Solid State Mater Sci* **41**(6): 447–481 (2016)

[9] Wakuda M, Yamauchi Y, Kanzaki S, Yasuda Y. Effect of surface texturing on friction reduction between ceramic and steel materials under lubricated sliding contact. *Wear* **254**(3–4): 356–363 (2003)

[10] Byun J W, Shin H S, Kwon M H, Kim B H, Chu C N. Surface texturing by micro ECM for friction reduction. *Int J Precis Eng Manuf* **11**(5): 747–753 (2010)

[11] Wang X L, Kato K. Improving the anti-seizure ability of SiC seal in water with RIE texturing. *Tribol Lett* **14**(4): 275–280 (2003)

[12] Stephens L S, Siripuram R, Hayden M, McCartt B. Deterministic micro asperities on bearings and seals using a modified LIGA process. In *Proceedings of ASME Turbo Expo 2002: Power for Land, Sea, and Air*, Amsterdam, The Netherlands, 2002: 573–580.

[13] Zavos A, Nikolakopoulos P G. Tribological characterization of smooth and artificially textured coated surfaces using block-on-ring tests. *FME Trans* **43**(3): 191–197 (2015)

[14] Raeymaekers B, Etsion I, Talke F E. A model for magnetic tape/guide friction reduction by laser surface texturing. *Tribol Lett* **28**(1): 9–17 (2007)

[15] Etsion I. State of the art in laser surface texturing. *J Tribol* **127**(1): 248–253 (2005)

[16] Siripuram R B, Stephens L S. Effect of deterministic asperity geometry on hydrodynamic lubrication. *J Tribol* **126**(3): 527–534 (2004)

[17] Marian V G, Kilian M, Scholz W. Theoretical and experimental analysis of a partially textured thrust bearing with square dimples. *Proc Inst Mech Eng, Part J: J Eng Tribol* **221**(7): 771–778 (2007)

[18] Yu H, Deng H, Huang W, Wang X. The effect of dimple shapes on friction of parallel surfaces. *Proc Inst Mech Eng, Part J: Eng Tribol* **225**(8): 693–703 (2011)

[19] Nanbu T, Ren N, Yasuda Y, Zhu D, Wang Q J. Micro-textures in concentrated conformal-contact lubrication: Effects of texture bottom shape and surface relative motion. *Tribol Lett* **29**(3): 241–252 (2008)

[20] Shen C, Khonsari M M. Effect of dimple's internal structure on hydrodynamic lubrication. *Tribol Lett* **52**(3): 415–430 (2013)

[21] Han J, Fang L, Sun J P, Wang Y Q, Ge S R, Zhu H. Hydrodynamic lubrication of surfaces with asymmetric microdimple. *Tribol Trans* **54**(4): 607–615 (2011)

[22] Schuh J K, Ewoldt R H. Asymmetric surface textures decrease friction with Newtonian fluids in full film lubricated sliding contact. *Tribol Int* **97**: 490–498 (2016)

[23] Lee Y H, Schuh J K, Ewoldt R H, Allison J T. Enhancing full-film lubrication performance via arbitrary surface texture design. *J Mech Des* **139**(5): 053401 (2017)

[24] Fesanghary M, Khonsari M M. Topological and shape optimization of thrust bearings for enhanced load-carrying capacity. *Tribol Int* **53**: 12–21 (2012)

[25] Shen C, Khonsari M M. Numerical optimization of texture shape for parallel surfaces under unidirectional and bidirectional sliding. *Tribol Int* **82**: 1–11 (2015)

[26] Lin C D, Lee Y H, Schuh J K, Ewoldt R H, Allison J T. Efficient optimal surface texture design using linearization. In *World Congress of Structural and Multidisciplinary Optimisation*, Braunschweig, Germany, 2017: 633–647.

[27] Zhang H, Dong G N, Hua M, Chin K S. Improvement of tribological behaviors by optimizing concave texture shape under reciprocating sliding motion. *J Tribol* **139**(1): 011701 (2017)

[28] Wang W, He Y Y, Zhao J, Li Y, Luo J B. Numerical optimization of the groove texture bottom profile for thrust bearings. *Tribol Int* **109**: 69–77 (2017)

[29] Wang W, He Y Y, Zhao J, Mao J Y, Hu Y T, Luo J B. Optimization of groove texture profile to improve hydrodynamic lubrication performance: Theory and experiments. *Friction*, in Press, DOI 10.1007/s40544-018-0247-1.

[30] Rahmani R, Mirzaee I, Shirvani A, Shirvani H. An analytical approach for analysis and optimisation of slider bearings with infinite width parallel textures. *Tribol Int* **43**(8): 1551–1565 (2010)

[31] Rahmani R, Rahnejat H. Enhanced performance of optimised partially textured load bearing surfaces. *Tribol Int* **117**: 272–282 (2018)

[32] Chen C Y, Liu C S, Li Y C, Mou S. Geometry optimization

for asymmetrical herringbone grooves of miniature hydrodynamic journal bearings by using Taguchi technique. *Proc Inst Mech Eng, Part J: J Eng Tribol* **229**(2): 196–206 (2015)

[33] Shinde A B, Pawar P M. Multi-objective optimization of surface textured journal bearing by Taguchi based Grey relational analysis. *Tribol Int* **114**: 349–357 (2017)

[34] Qiu M F, Delic A, Raeymaekers B. The effect of texture shape on the load-carrying capacity of gas-lubricated parallel slider bearings. *Tribol Lett* **48**(3): 315–327 (2012)

[35] Qiu M F, Minson B R, Raeymaekers B. The effect of texture shape on the friction coefficient and stiffness of gas-lubricated parallel slider bearings. *Tribol Int* **67**: 278–288 (2013)

[36] Fu G, Untaroiu A. An optimum design approach for textured thrust bearing with elliptical-shape dimples using computational fluid dynamics and design of experiments including cavitation. *J Eng Gas Turbines Power* **139**(9): 092502 (2017)

[37] Ramesh A, Akram W, Mishra S P, Cannon A H, Polycarpou A A, King W P. Friction characteristics of microtextured surfaces under mixed and hydrodynamic lubrication. *Tribol Int* **57**: 170–176 (2013)

[38] Lu X B, Khonsari M M. An experimental investigation of dimple effect on the Stribeck curve of journal bearings. *Tribol Lett* **27**(2): 169–176 (2007)

[39] Johnston M T, King W P, Ewoldt R H. Shear stress characteristics of microtextured surfaces in gap-controlled hydrodynamic lubrication. *Tribol Lett* **82**: 123–132 (2015)

[40] Kango S, Singh D, Sharma R K. Numerical investigation on the influence of surface texture on the performance of hydrodynamic journal bearing. *Meccanica* **47**(2): 469–482 (2012)

Nilesh D. HINGAWE. He received his master degree in mechanical engineering in 2015 from Shivaji University, Kolhapur, India. He is studying for his Ph.D. degree at the Mechanical Engineering Department, Motilal Nehru National Institute of Technology Allahabad, India. His research interests include tribology, bearings, and surface texturing.

Skylab P. BHORE. He received his Ph.D. in mechanical engineering from Indian Institute of Technology Delhi, India, in 2015. He works as an assistant professor at Motilal Nehru National Institute of Technology Allahabad, India. His research areas are rotor dynamics, air lubrication, tribology, and micro-electromechanical systems (MEMS).